Nuclear Engineering and Technology 57 (2025) 103599

Contents lists available at ScienceDirect

Nuclear Engineering and Technology

journal homepage: www.elsevier.com/locate/net

Original Article

Floor response characteristics of NPP auxiliary building subjected to bi-directional ground motions

Bidhek Thusa [a], Duy-Duan Nguyen [b], Md Samdani Azad [c], Tae-Hyung Lee [d,*]

[a] Department of Civil and Environmental Engineering, Hanbat National University, Daejeon, South Korea
[b] Department of Civil Engineering, Vinh University, Vinh, 461010, Viet Nam
[c] Department of Civil and Environmental Engineering, Yonsei University, Seoul, South Korea
[d] Department of Civil and Environmental Engineering, Konkuk University, Seoul, 05029, South Korea

ARTICLE INFO

Keywords:
Auxiliary building
Multi-layer shell model
Bi-directional motions
Floor response spectrum
Time-history analysis

ABSTRACT

The objective of this study is to investigate the seismic floor response characteristics at critical locations of the auxiliary building (AB) of a nuclear power plant. AB is so irregular that floor responses at different locations are expected to be different even at the same floor. Time history analyses are performed for a finite element model of AB for various bi-directional ground motions. It is observed that floor response spectra at 12 distinct locations are significantly different. The bi-directional effect is observed to be 24 %–42 % higher when compared to uni-directional cases. The response trajectory due to bi-directional motions shows the major direction of response are variable and solely depends on the ground motion properties suggesting the current analysis techniques being viable for over/under estimation of floor responses. The critical angle of incidence for AB is found to be 105°. Hence, this study also suggests virtually dividing a floor into several groups based on their seismic response characteristics for an efficient evaluation of the seismic performance of large structures like AB.

1. Introduction

Auxiliary building (AB) is the largest structure associated with NPP structures. AB houses most of the NPP equipment and safety systems of the reactor such as radioactive waste systems, emergency cooling water systems, chemical and volume control systems, and heat exchanger generators. Nuclear energy is one the cleanest energy sources attracting many developed nations as the power generation in NPP causes one of the lowest levels of fatalities per unit of energy generated in comparison to other sources of energy. However, it can be potentially hazardous if the structure is exposed to accidents like Chernobyl (Ukraine,1986) and Fukushima Daiichi (Japan 2011). Moreover, the uncertainties due to earthquakes are always huge concerns for the safety of NPP structures which knock the researchers for the necessity of study of seismic performance evaluation of NPP structures and components. For seismic performance evaluations, NPP structures are normally modeled in terms of the lumped-mass stick model (LMSM) or three-dimensional finite element model using solid elements (3D FEM). LMSM simplifies the real structures to linear-elastic beam elements with concentrated masses at nodes. This modeling approach has been widely applied for seismic response analyses and vulnerability assessments of NPP structures [1–15] and equipment [16–19]. In addition to LMSM and 3D FEM, the shell element model can be used for structural response analyses of nuclear engineering structures. Some studies utilized a linear shell model [20–23] to facilitate numerical simulations. Besides, a multi-layer shell model (MLSM) considering the nonlinearity of materials was also applied to perform the behaviors of the NPP structures under internal pressures [24] and earthquakes [25–28]. The AB is a simple but massive critical shear wall structure in NPP structures. A full scale [29] and scaled model of RC NPP model with both containment and AB [30] was previously studied for safety and damage assessment under aircraft impact loading. Overall, for evaluating the seismic response of structures, the floor responses are recorded on a specific node, and the floor is considered to behave rigidly through the assignment of a rigid diaphragm. Furthermore, most of studies conducted on NPP structures are focused on RCB, while seismic performance studies of a full-scale structure of AB are still extremely limited due to computational limitations.

In the case of seismic bi-directional effect, several studies [31–34] have indicated that a structure can experience complex as well as significant amplification in seismic damage when subjected to seismic bending about both of its principal axes in comparison to the uniaxial

* Corresponding author.
E-mail address: thlee@konkuk.ac.kr (T.-H. Lee).

https://doi.org/10.1016/j.net.2025.103599
Received 10 July 2024; Received in revised form 14 January 2025; Accepted 20 March 2025
Available online 22 March 2025

interaction. In the US, the regulatory seismic codes require at least two sets of horizontal ground motion components for 3D response history analysis of building structures in both the design and evaluation of existing structures. The parametric study conducted by USGS [35] suggests that the ground motion rotated on the maximum direction or fault-normal/fault parallel direction doesn't necessarily provide the most critical engineering demand parameters (EDPs) in the nonlinear-inelastic domain, however, they tend to produce larger EDPs than as recorded (arbitrarily oriented) motions. A study on maximum spectral demand in the near-fault region showed a clear dependence on the period of earthquake motion and Somerville directivity parameters (i.e., strike-slip and dip-slip) [36]. Furthermore, recent studies [37,38] of the directivity effect of bi-directional ground motion in base-isolated structures added further importance to the consideration of bi-directional ground motion for the seismic performance of critical structures. Mostly, studies conducted on the bi-directional effect of motions are focused on the field of building and simple structures [31–38]. However, the study on the effect of bi-directional ground motion in a three-dimensional FEM model of AB of NPP is almost negligible and very limited.

This study aims to explore the floor response characteristics of AB under bi-directional ground motions. A set of 40 input ground motions is selected from the PEER center database to perform time-history analyses. For a clearer illustration on load directivity effect, the first set of 40 input motions is utilized to perform time history analyses along the horizontal directions (i.e. X- and Y- direction). The FRS along both the X and Y-directions of the structure due to the uni-direction motions is investigated. Whereas, in the second case, for proper study of bi-directional seismic input effect, a set of 15 bi-directional motions are selected for the investigation of floor response characteristics of AB due to bi-directional input motions. The 15 bi-directional motions are selected in a way that the motions hold an almost close response spectrum along X and Y-directions. The seismic response of AB is measured in terms of FRS which is considered one of the critical EDPs in the seismic performance evaluation of structures.

2. Numerical modeling of the auxiliary building

2.1. Structural configuration of auxiliary building

AB of a nuclear power plant was adopted for the numerical analysis of this study. The plan dimension of AB adopted for this study is 104.85 m in length along the longitudinal axis and 102.4m on the transverse axis (Fig. 1). AB is a shear wall building consisting of nine floors with variable floor heights according to the installed NPP control systems. The physical characteristics and floor levels of AB are presented in Tables 1 and 2, respectively. The shear wall elements of AB have various thicknesses with the thickest section as the external wall. For clarity, we have categorized the shear walls of AB into various groups according to the thickness and purpose of the wall. The section and reinforcement details of several wall sections are listed in Table 3.

Table 1
Physical properties of the structures.

Description	Details
Total length	104.85 m
Total breadth	102.4 m
Total height	48.742 m
Foundation type	Raft foundation
Structural configuration type	RC shear wall structure
Reinforcement layers	Max 6 layers, Min 2 layers
Major irregularity	Large central void of 48 m diameter
Vertical irregularity	Decrease in floor area for each floor above
Numerical modeling type	Multi-layer shell model

Table 2
Floor levels of the investigated AB.

Floor	Floor height (m)	Floor elevation (m)
Ground floor (B2)	7.06	0
First floor (B1)	6.812	7.06
Second floor	6.096	13.872
Third floor	5.334	19.968
Fourth floor	5.6388	25.302
Fifth floor	4.8762	30.941
Sixth floor	5.487	35.817
Seventh floor	2.438	41.304
Eighth floor	4.7248	43.742
Ninth floor		48.4668

Table 3
Shear wall section details.

SN	Description	Thickness (m)	Vertical reinf.	Horizontal reinf.	No. of reinf. layers
1	External wall (W1)	1.27	#14@305 mm	#11@305 mm	4
2	Internal wall (W2-1)	1.27	#14@228.6 mm	#11@228.6 mm	4
3	Internal wall (W2-2)	1.27	#14@228.6 mm	#11@228.6 mm	6
4	Internal partition wall (W3)	0.863	#11@305 mm	#10@305 mm	4
5	Internal partition wall (W4)	0.76	#11@305 mm	#10@305 mm	4
6	Internal partition wall (W5)	0.54	#10@228.6 mm	#10@305 mm	2
7	Internal partition wall (W6)	0.54	#11@228.6 mm	#11@305 mm	2

2.2. Finite element modeling

The numerical model of containment building is developed in SAP2000 [39] using MLSM. The shell element is divided into several layers with different thicknesses. Each layer represents a specific material in which reinforcement and concrete layers are set up together, as shown in Fig. 2. Material properties are assigned to corresponding layers, in which the nonlinearity is considered in material models, as shown in Fig. 3. The floor load of 11.97 kN/m^2 is applied to the floors where the equipment and control systems reside. Furthermore, a rigid diaphragm is considered on each floor of AB.

The shell element is a type of surface element used to model membrane, plate, and shell behavior. The shell element can be layered through the thickness to consider the out-of-plane bending of a composite section. The multi-layer shell element is theoretically derived from the principles of composite material mechanics. This kind of element can simulate the interaction between in-plane and out-of-plane responses and the in-plane flexural-shear behaviors of RC walls [40–42]. For each of the in-plane integration points, a layered/composites integrated section is implemented to account for the nonlinear behavior of reinforced concrete. This element simplifies the three-dimensional nonlinear behavior of the shear walls to a shell situation by discretizing them into several fully bonded layers in the thickness direction.

The limitations of the shell element are inability to address the transverse shear stresses and through-thickness effects. However, ease in mesh creation and significant reduction of computational cost make MLSM more feasible for simulation of large structures like AB in comparison to LMSM and solid 3D FEM model (Nguyen et al., 2021). Hence, MLSM provides a broader range of applications in structural engineering for the simulation of RC shear-walled structures.

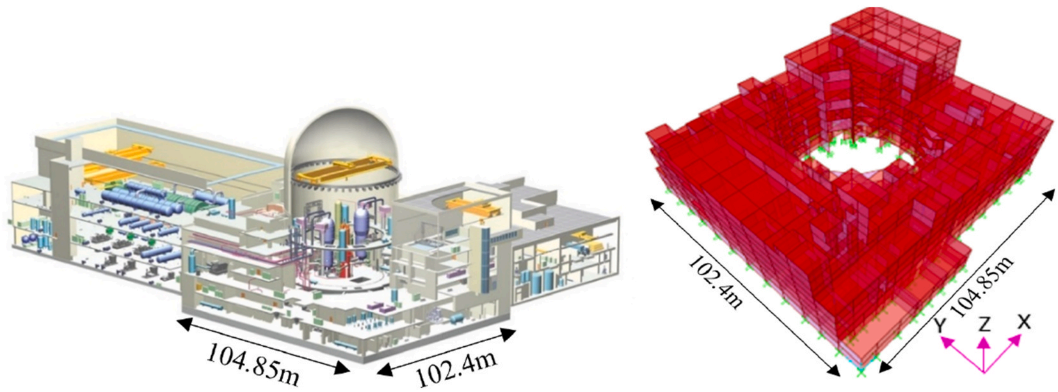

Fig. 1. General view (left) of NPP and AB (right).

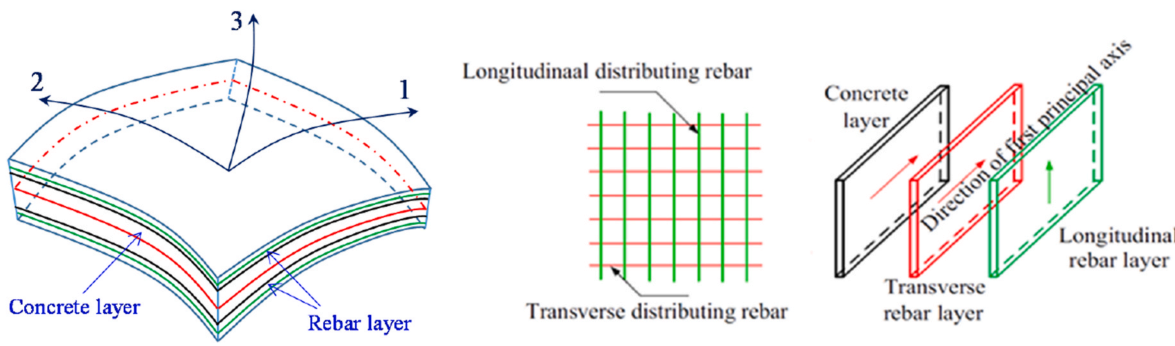

Fig. 2. Illustration of MLSM.

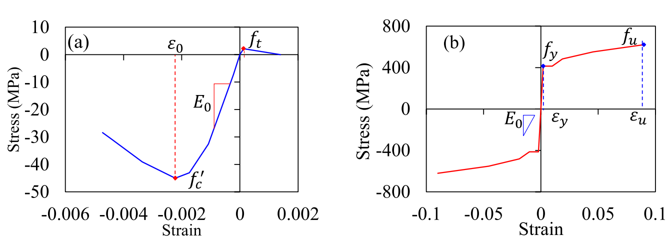

Fig. 3. Nonlinear material models for MLSM: (a) concrete and (b) reinforcing bars.

The details of material properties for reinforcing bars and concrete are presented in Table 4 in which nonlinear characteristics of materials are presented in Fig. 3. Based on these input parameters, we expect that MLSM can approximate the nonlinear behaviors of the structure accurately. This MLSM can be a promising approach in terms of computation for analyzing large structures like AB as this numerical model significantly reduces the number of degrees of freedom compared to the Solid FEM approach. This study selected a 2-m mesh size containing 39,381 shell elements through a mesh convergence test conducted in by the first author [43]. It should be noted that AB is constructed in an extremely thick raft foundation due to its criticality. Hence, the boundary condition of AB is assumed to be fixed at the bottom.

Table 4
Mechanical properties of the material model of AB.

Material	Compressive strength (MPa)	Tensile strength (MPa)	Yield strength (MPa)	Ultimate strength (MPa)	Elastic modulus (MPa)
Concrete	45	2.18	–	–	32,000
Reinforcement	–	–	400	600	200,000

2.3. Eigenvalue analysis

Eigenvalue analysis is conducted to obtain the mode shapes and modal vibration frequency of the AB. Fig. 4 shows four typical mode shapes of the structure. The mass participation ratios for the first two fundamental modes based on translation in X- and Y-dir are 44 % and 69 %, respectively. It should be noted that the result of eigenvalue analyses reveals that AB is a stiff structure.

3. Seismic performance evaluation

3.1. Overview

Linear dynamic analyses in AB were carried out by imposing ground motion on both X and Y- directions, one at a time. The Newmark method with $\alpha = 0.5$ and $\beta = 0.25$, yields the constant average acceleration method (i.e., middle point rule) for solving the equation of motion in dynamic analyses.

The FRS, one of the most critical structural outputs, is monitored for investigating the seismic performance of AB. Numerous safety systems of the reactor like the radioactive waste system, emergency cooling water system, chemical control system, as well as several devices and relays, including electrical, electronic, and mechanical components, are attached to this structure at various levels and locations. The seismic responses of all the safety systems and their equipment along with devices are generally evaluated by using FRS. Seismic responses at twelve distinct locations on each floor, as shown in Fig. 5, were investigated in this study. The twelve distinct locations are selected based on the locations where the structure is highly likely to amplify in seismic response like corners, edges, or center of floors, and the location of major nonstructural components. Hence these locations play a critical role in the investigation of the seismic response of the AB.

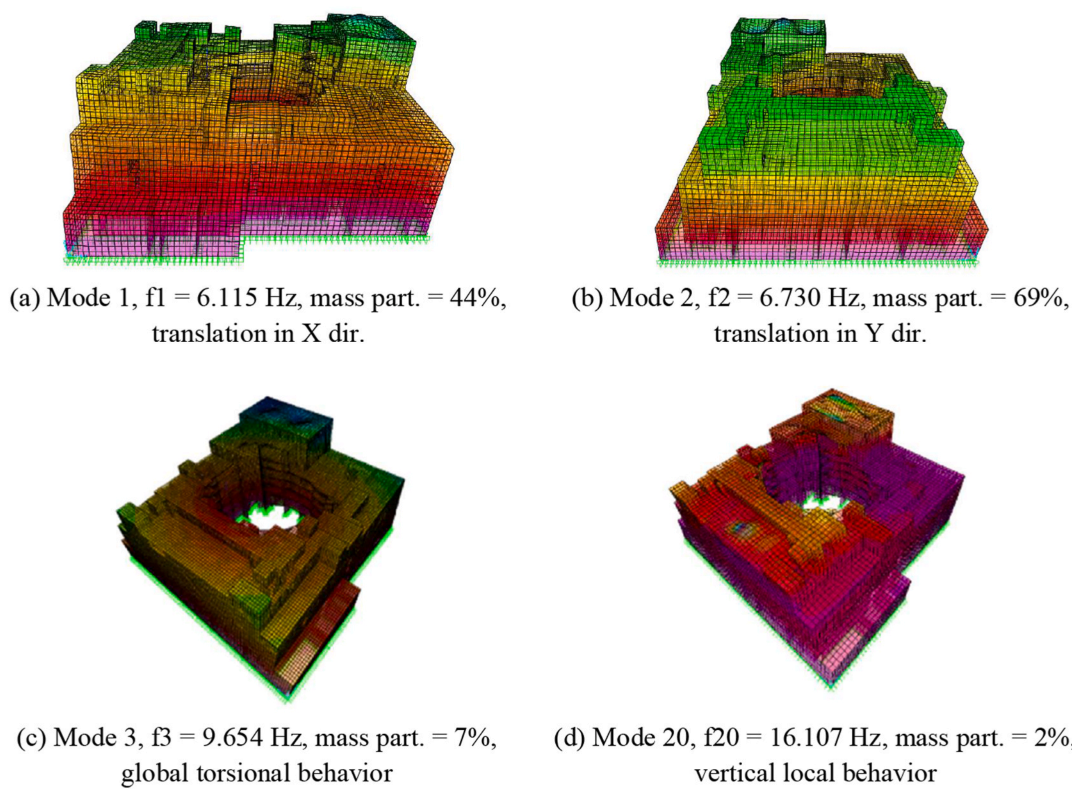

Fig. 4. Eigenvalue analysis results.

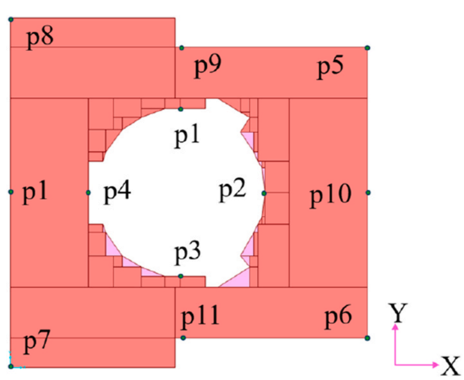

Fig. 5. Twelve seismic response recorder locations.

3.2. Rayleigh damping

Rayleigh damping model is commonly used in dynamic analyses, as expressed in the following form,

$$[C] = a[M] + b[K] \tag{1}$$

where $[C]$ is the damping matrix; $[M]$ and $[K]$ are the mass and stiffness matrices, respectively. a and b are the proportional damping coefficients, given by

$$a = \xi \frac{2\omega_i \omega_j}{\omega_i + \omega_j}; \ b = \xi \frac{2}{\omega_i + \omega_j} \tag{2}$$

where ω_i and ω_j are the circular frequencies of the predominant modes, which are the third and the fourth modes for MLSM, respectively; ξ is the damping ratio, set to 5 %. Hence the mass proportional coefficient (a) and stiffness coefficient (b) damping factors are calculated as 2.0442 and 1.210E-3, respectively.

3.3. Uni-directional seismic response

3.3.1. Input uni-directional ground motions

The NPP structures have been seismically designed using the US NRC 1.60 spectrum [44,45] with a PGA of 0.3g at the safe shutdown earthquake level. This study uses a set of 40 natural ground motions with mean response spectra as the NRC 1.60 design spectrum to conduct time-history analyses, as shown in Fig. 6. The ground motion records are selected from worldwide historical earthquakes, which are provided in the PEER center database [46].

3.3.2. X-direction

In the first set of studies, the input earthquake load is applied along the X-direction only. FRS of four extremities (p1, p2, p3, and p4) of RCB which have close contact with the AB were investigated when the earthquake is applied along the X-direction. The mean seismic response spectrum of the first set of locations (p1-4) in selected floors of the AB is presented in Fig. 7. It is observed that the results are consistent and there are a significant number of discrepancies between the seismic response of each location of four extremities. Location p3 has the lowest seismic response on all the floors whereas location p1 has the highest peak

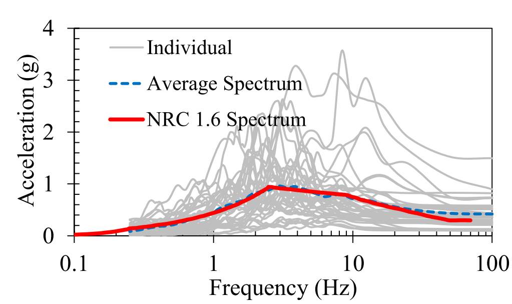

Fig. 6. Input ground motions.

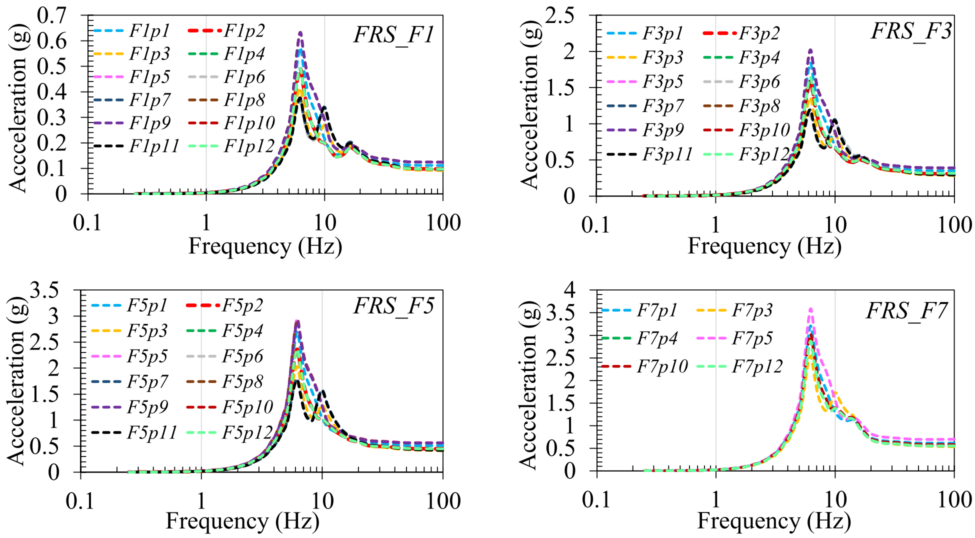

Fig. 7. Mean FRS due to X direction motion for each floor at all the locations p1-p12.

response among these four locations which is around 33 % higher response than that of p3. The response at p2 and p4 are around 16–18 % higher than that of p3 respectively in all floors. This shows that there are significant fluctuations in the floor response of AB.

Furthermore, the 2nd set of locations at the four edge corners of the floor is represented by p5, p6, p7, and p8 as shown in Fig. 7. From the mean FRS of these locations, it can be observed that the responses of p5 and p8 are almost identical, while p6 and p7 showed the same behavior. This means the response of each corner which is aligned with the direction of the application of earthquake load shows the same response. Moreover, the response in p5 and p8 is around 56.74 % higher than that of p6 and p7. AB is irregular in the vertical direction. Hence, all the 12 study locations do not continue up to the top floor. Additionally, there is the existence of large voids in floors to accommodate equipment as well as RCB. Consequently, the torsional behavior is more dominant in AB due to vertical structural irregularities. Therefore, a higher response in the locations p5 and p8 is observed. This is because p5 and p8 extend up to the 9th floor increasing mass along this area.

Finally, the 3rd set of locations is the middle locations of each side of AB represented as p9, p10, p11, and p12 are presented in Fig. 7. It shows the mean FRS plot for the 3rd set of locations (i.e., p9, p10, p11, p12). Three different peaks are observed for each floor. The largest peak is from the response of location p9 which is around 57 % higher than that of p11. While the responses of p10 and p12 have almost similar responses on every floor. The peak response at p10 and p12 is around 28.41 % higher than the peak response at p11.

The comparison of mean FRS for all 12 locations is shown in Fig. 7. It is observed that all the FRS is amplified at the fundamental frequency of AB (i.e., 6.115 Hz). Five distinct groups of peak response are observed in all locations on each floor. The first one is the highest peak response comprising the response of p5, p8, and p9 approximately 56 %–58 % higher than the lowest peak response attributed by the lowest response group (i.e., the response of p6, p7, and p11). Secondly, p1 gives the second highest peak which is around 32 %–35 % higher than that of the lowest response group (i.e., the response of p6, p7, and p11). The third group is the responses of p2, p4, p10, and p12, which showed a 16 %–18 % increment in seismic response compared to that of the lowest response group. The fourth response group consists of responses of p3 which are around 8 %–13 % higher than that of the lowest response group. All these five response groups lie in five different alignment groups along the direction of the applied earthquake load as shown in Fig. 8.

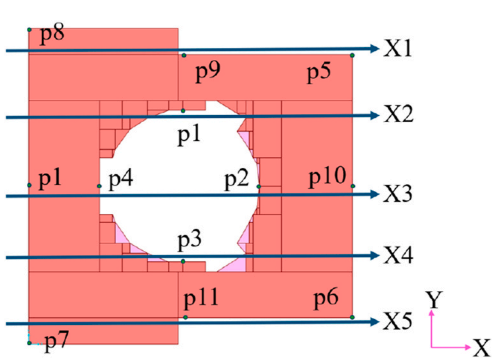

Fig. 8. Response alignment lines of AB along the X-direction earthquake.

Fig. 8 presents the five alignment groups categorized according to the alignment of twelve nodes along the X-direction earthquake load. The observed five different peaks lie along each alignment from X1 to X5. It is observed that the locations along X1 showed the highest peak floor response while it decreases as we move from X1 to X5. X1 consists of 3 locations i.e., p5, p8, and p9. Similarly, X2, X3, X4, and X5 consist of locations as shown in Fig. 8. The nodes located on alignment X5 have the lowest peak floor responses. The floor response along the alignments corresponds to the response of nodes along each alignment which is the floor response presented in Fig. 7. The lowest peak response shown by X5 can be due to the floor load and mostly due to vertical irregularity of the structure. Thus, this variation of floor response on the overall floor is due to the dominant torsional behavior of the AB, which is caused by the vertical irregularity of the structure.

3.3.3. Y-direction

In the second phase of the study, the same earthquake load is applied along the Y-direction to investigate the structural sensitivity of the direction of the earthquake load. The FRS for all the three sets of locations i.e. interior extremities of RCB (p1, p2, p3, and p4), four outer corners (p5, p6, p7, and p8), and middle location of each face of AB (p9, p10, p11, and p12) were investigated. The mean seismic floor response spectrum of all the locations on selected floors (F1, F3, F5, and F7) is presented in Fig. 9. It is observed that the results are consistent and behave in a similar pattern as discussed in the earlier section when the earthquake load is in the X-direction. However, the variation of floor response is lesser in comparison to that due to X-direction motion on each of the floor response alignment lines (i.e., X1 to X5). The peak of FRS at the locations p5, p10, and p6 is the lowest on all floors, whereas FRS at p8, p7, and p12 has the highest peak around 10–20 % higher

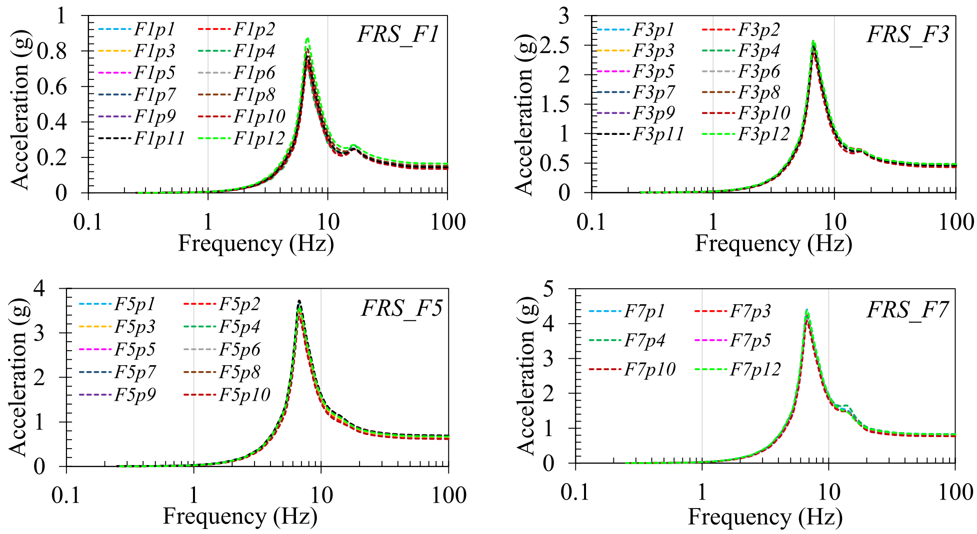

Fig. 9. Mean FRS due to Y-direction motion for each floor at all the locations p1-p12.

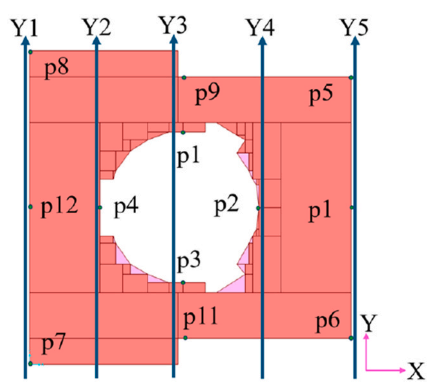

Fig. 10. Response alignment lines of AB along the Y-direction earthquake.

response than that of the lowest response. The response at location p2 is 2–3 % higher, while the response at p1, p3, p9, and p11 are around 5–10 % higher than the lowest response respectively in all floors. Similarly, response at p4 ranges from 10 to 13 % higher than the minimum value. The results from the Y-direction motion also validated that there are significant fluctuations in the floor response of AB. In addition to this, the magnitude of the response amplification is higher for the case due to X direction motion than that due to Y direction motions.

Fig. 10 presents the alignments along the Y-axis of AB, where Y1, Y2, Y3, Y4, and Y5 are the groups categorized according to the FRS response alignment of twelve nodes along the Y-direction. The locations along Y1 showed the highest peak response, while locations along Y5 showed the lowest response.

3.4. Bi-directional seismic response

3.4.1. Input bi-directional ground motion

A set of 15 bi-directional ground motions are selected from the PEER center database [45]. The selection is carried out in such a way that the mean spectra of the 15 motions match with the NRC 1.60 design spectrum for performing time history analysis. Fig. 11 represents the response spectrum of the bi-directional motion along the X and Y-direction.

3.4.2. Seismic response due to bi-directional motions

The resultant response quantity due to bi-directional ground motions is calculated by using the well-known SRSS combination rule. Fig. 12 represents the resultant response on each location due to bi-directional motion. The variation of floor response due to bi-directional motions also shows a similar pattern as discussed in earlier sections. The 5 variation patterns are represented as R_{XY} 1 – R_{XY} 5 in Fig. 13, which is similar in nature to the response presented in Figs. 8 and 10. The highest peak response lies with R_{XY} 1 and subsequently it decreases to the lowest peak response along R_{XY} 5. The peak response on the location along R_{XY}1 is 25 %–30 % higher than that of the lowest peak response along R_{XY}5. While the response along R_{XY}2 is around 20 % higher than the minimum response at location 6. Similarly, responses along R_{XY}3 are 8 %–16 % than that of R_{XY}5. Also, peak response along R_{XY}4 is around 5 % higher than that of R_{XY}5.

Figs. 14 and 15 represent the comparison of the floor responses due to uni-directional motion and bi-directional motion at the two locations (i.e., P5 and p10) which lie on the top floor. In addition, the resultant response due to bi-directional motion is also presented. The magnitude of the resultant response due to bi-directional motion is increased by 32 % than the response due to uni-directional motion at location 5 of the

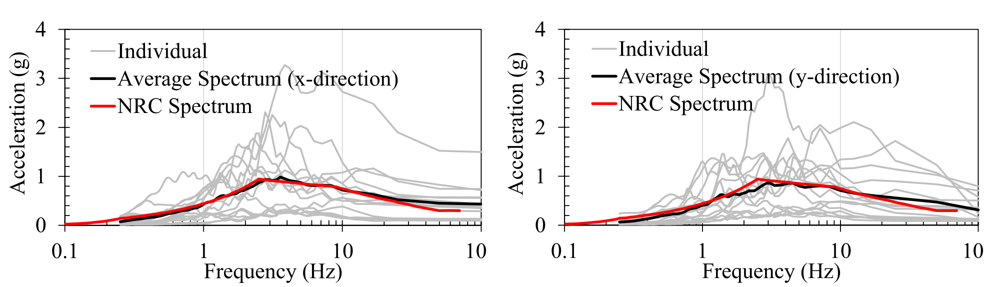

Fig. 11. Input bi-directional motions.

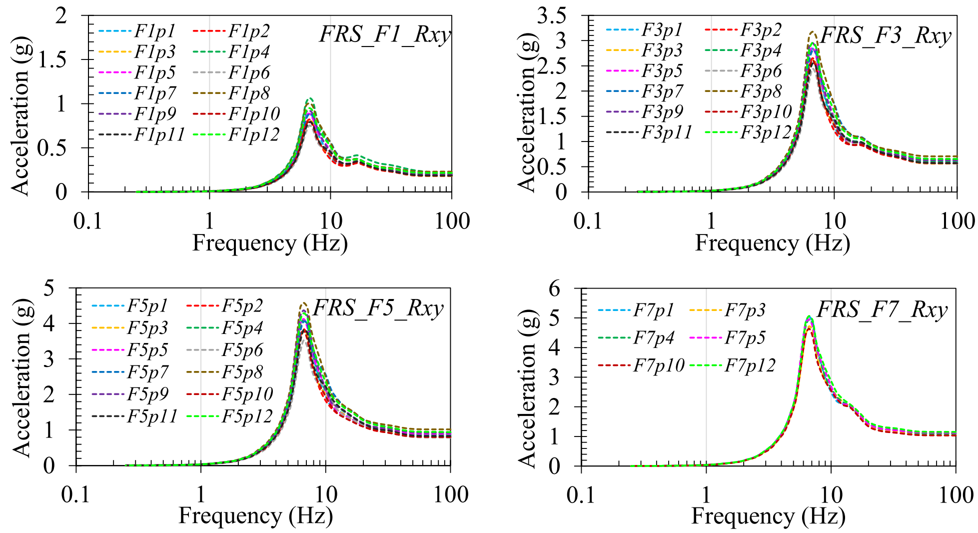

Fig. 12. Resultant FRS due to bi-direction motion for each floor at all the locations p1-p12.

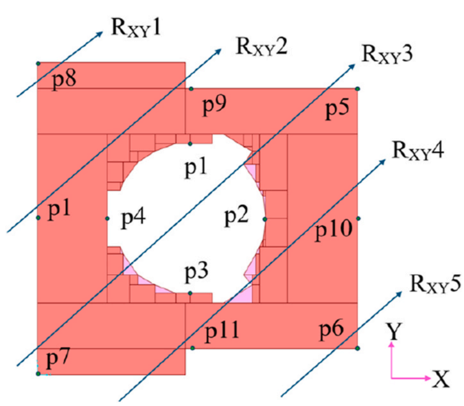

Fig. 13. Response alignment lines for resultant response due to bi-directional motion.

top floor. The resultant response due to bi-directional motion at location 10 is increased by 42 % than the response due to Y-direction motion and is increased by 24 % than the response due to X-direction motion which is presented in Fig. 15. Most importantly, the resultant response due to bi-direction motion is amplified by more than 24 % in all the locations than response due to uni-directional motion, which argues the importance of consideration of seismic impact in AB due to bi-direction motion.

3.5. Effect of ground motion angle of incidence for AB

The critical ground motion angle of incidence for a structure is determined by the application of the bi-directional ground motion applied at several angles of incidence with respect to the structural axes. The most commonly used method for considering angle of incidence of a ground motions is by rotating the bi-directional ground motion components maintaining the global axes of the structural model as constant. The bi-directional components of the ground motion are recalculated using linear transformation and applied to the global axes of the structure. This study considered rotating the bi-directional components from 0° to 360° at an interval of 15° increments from the 15 different ground motions.

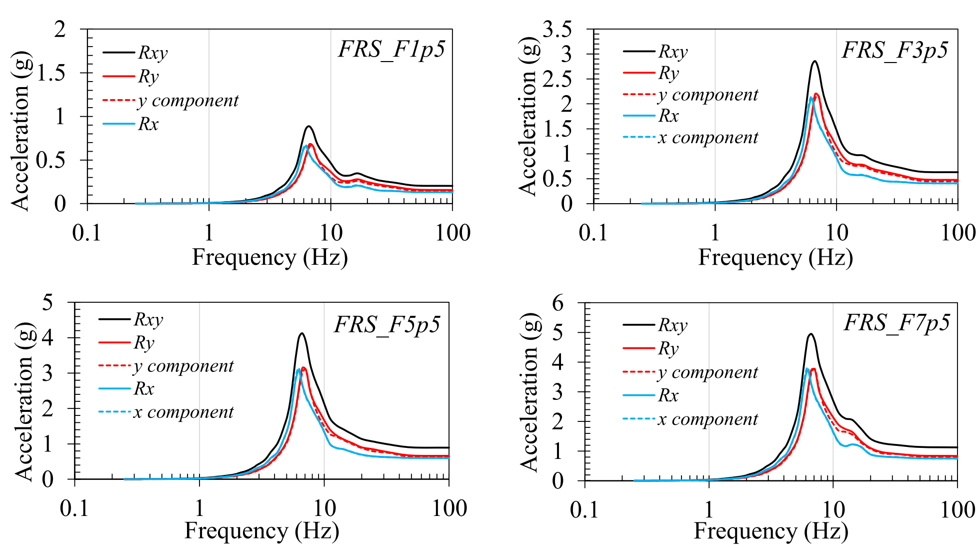

Fig. 14. Resultant FRS to bi-direction motion for each floor at all the locations p5.

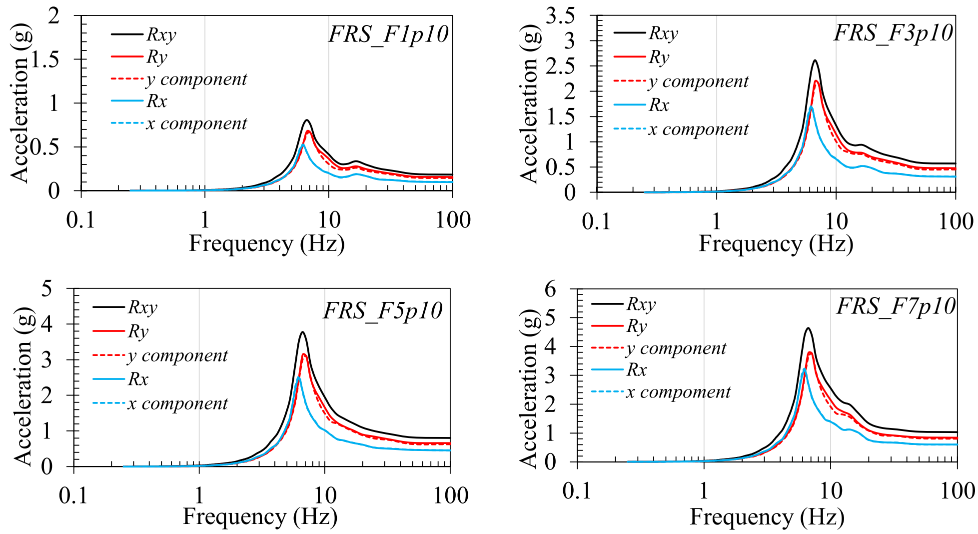

Fig. 15. Resultant FRS to bi-direction motion for each floor at all the locations p10.

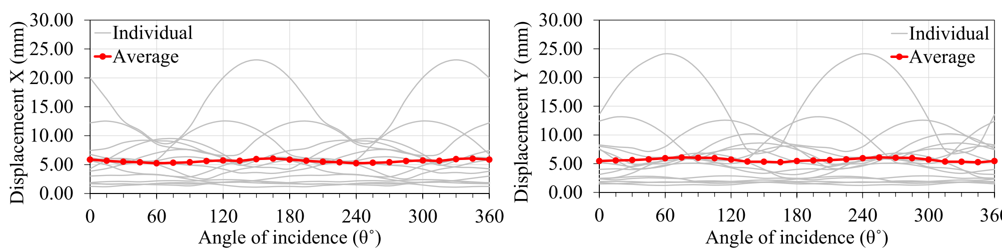

(a) along X axis

(b) along Y axis

Fig. 16. Peak displacement at top node.

3.5.1. Peak displacement demand for AB

Displacement demand is one of the important response parameters while conducting seismic performance evaluation. The peak displacement at the top node on each response axes of AB due to each input bi-directional ground motions and its angle of incidence is presented in Fig. 16. The peak displacement response obviously depends upon the input ground motion which can be observed from Fig. 16. There is no unique orientation for AB to have maximum the demand, the demand is completely related to each input ground motion properties. The peak displacement demand is observed to be close to 25 mm while the average peak displacement is around 5.5 mm along both axes.

3.5.2. Peak acceleration demand for AB

The peak acceleration demand for AB due to bi-directional ground motion at various angles of incidence is presented in Fig. 17. The peak acceleration demand shows similar behavior to the peak displacement response. The average peak acceleration demand is around 1.0g along both axes. It is observed that the peak acceleration due to various angles of incidence also varies with input bi-directional ground motions. Hence, it is concluded that the structural demand of AB is significantly dependent on the input ground motion properties.

3.5.3. Shear force demand for AB

The base shear provides the maximum lateral force in the structure due to an earthquake. The performance of a structure depends on the base shear capacity. The peak base shear of AB due to bi-directional motion at various angles of incidence is presented in Fig. 18. The peak base shear demand of AB is observed to be 6580 MN along the Y axis while having 5090 MN along the X axis. The result represents a similar nature to other demand parameters discussed earlier.

3.5.4. Critical ground motion angle of incidence for AB

The critical ground motion angle of incidence is very important for seismic performance evaluation due to bi-directional ground motions as

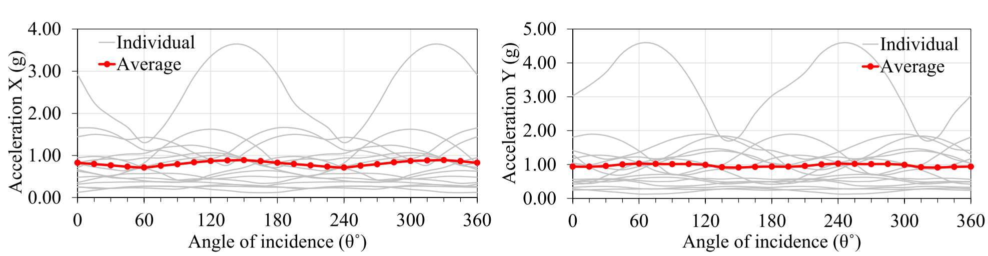

(a) along X axis

(b) along Y axis

Fig. 17. Peak acceleration at top node.

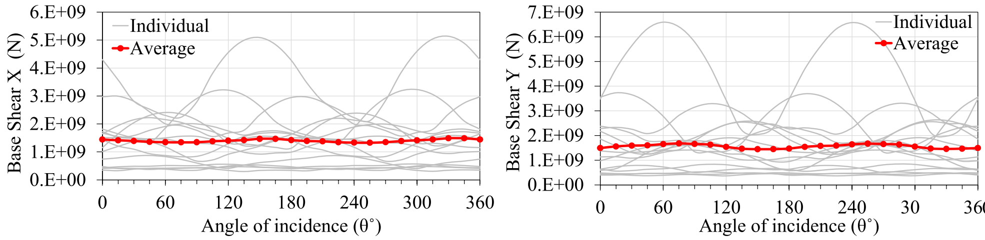

(a) along X axis (b) along Y axis

Fig. 18. Peak base shear.

it provides the maximum demand based on the specific angle of incidence. The average peak demands due to 15 bi-directional ground motions at various angles of incidence is presented in Fig. 19. Fig. 19a represents the average peak displacement demand of AB along both axes and the resultant. It is observed that the average peak displacement demand along X axis decreases from 0° to 105° and increases from 105° to 180°, while it is symmetric for the other remaining angle of incidence. For the case of Y axis, the average peak displacement increases from 0 to 105 and decreases from 105° to 180° with the remaining demand as symmetric in nature. The average peak resultant displacement demand is observed to be decreased from 0 to 60 followed by increase from 60 to 135 while 135 to 180 in decreasing other. The average peak displacement due to remaining angles to be symmetric. The observation for average peak acceleration demand present in Fig. 19b is similar to the displacement demand. The average peak base shear demand presented in Fig. 19c shows that the base shear demand decreases from 0 to 105 followed by an increase from 105 to 180 along X-axis, while it increases from 15 to 120 and decreases from 120 to 180 along Y-axis. For the case of the average peak resultant base shear demand, it increases from 15° to 105° and decreases from 105° to 180° angle of incidence following the symmetric response for 180° to 360°. The observations of the critical angle for displacement and acceleration are similar while the observations for base shear showed minor deviation which is due to the location of the top node. The top node lies at the location p5. From the observation of average peak resultant demands, the maximum average peak demand lies at 105° for displacement and acceleration, while the maximum average peak base shear demand lies at 75°, 90°, and 105° angle of incidence. Therefore, the critical angle of incidence for AB is 105°.

3.5.5. *Alternative approach for critical angle of incidence*

Furthermore, the bi-directional trajectory of output response is presented in Fig. 20. The output response trajectory shows varying major axes for different motions which are based on the directional properties of the ground motion. It should be noted that the bi-directional ground motion should be applied at various angles with respect to the structural axes to cover all the possible responses, which is not practical [35]. This leads this section to investigate the effect of bi-directional ground motions with the angle of incidence of zero degrees with structural axes and investigate the bi-directional response trajectory to make it computationally more feasible. This study provides the major axis of response for AB when the angle of incidence is zero-degree. The trajectories of 3 motions are presented in Fig. 20 for the sake of space. The observed direction of major response axis due to all the input bi-directional ground motion is listed in Table 5. This follows that there is no unique orientation for the given structure maximizing EDPs, the peak values are independent of the ground motions and its rotation angles [35].

However, the average response trajectory of the 15 input bi-directional ground motions from Table 5 is 106.799°, which is very close to 105° critical angle of incidence for average peak displacement and acceleration demand from Section 3.5.4. Hence, this alternative approach can be utilized for large structures like AB for seismic performance evaluation due to bi-directional ground motions for reducing significant amount of computational cost.

4. Conclusions

This study investigates the floor response characteristics of AB of a nuclear power plant. The nonlinear FEM model of AB is developed by using multi-layer shell elements. A series of linear time series are performed for various bi-directional ground motions. The seismic floor response is studied for the various critical locations along various alignments on each floor. Due to the high computational cost of AB, this study is limited to linear time history analysis. The following conclusions can be drawn based on the output of numerical analyses.

- For massive structures like AB having vertical irregularity, torsion can be the most critical mode of vibration.

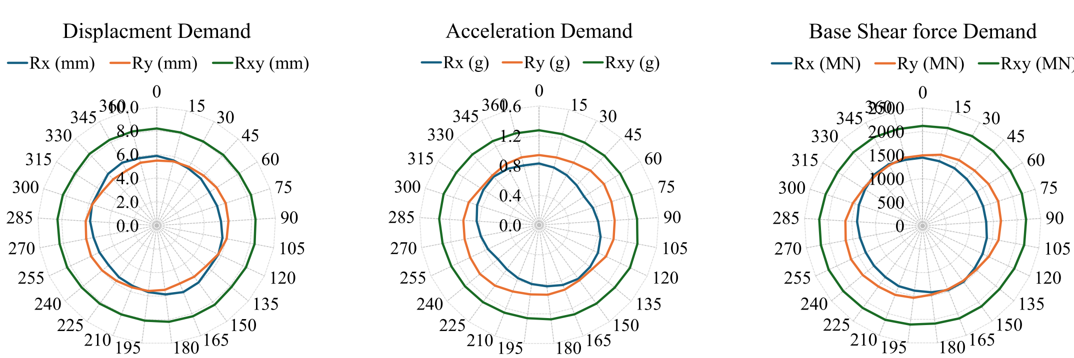

(a) (b) (c)

Fig. 19. Average peak demand: (a) Displacement, (b) Acceleration, and (c) Base shear.

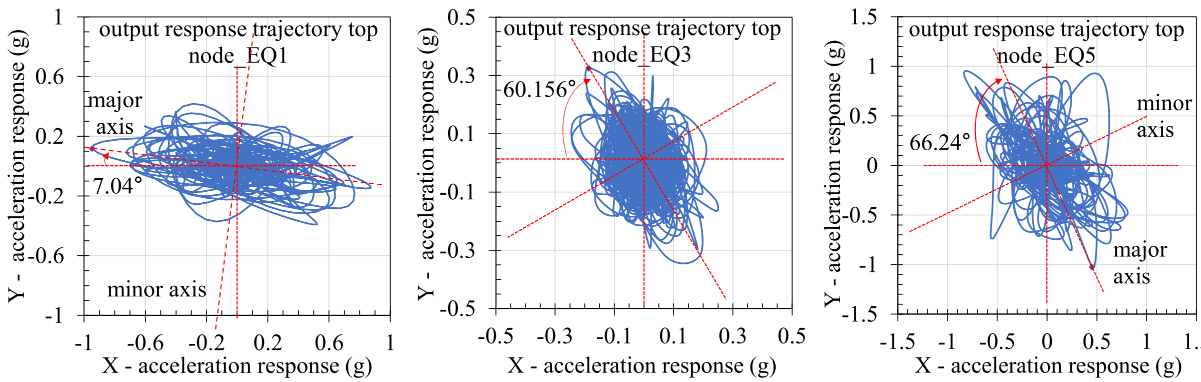

Fig. 20. Bi-directional trajectory of output response.

Table 5
The direction of the major response axis.

Ground motion	Direction of the major response axis with respect to the structural X-axis (clockwise)	Direction of the major response axis with respect to structural Y-axis (clockwise)
EQ1	7.040°	97.040°
EQ2	9.591°	99.591°
EQ3	60.156°	150.156°
EQ4	87.305°	177.305°
EQ5	66.240°	156.240°
EQ6	67.554°	22.446°
EQ7	12.988°	102.988°
EQ8	31.942°	121.942°
EQ9	64.930°	25.070°
EQ10	66.820°	23.180°
EQ11	60.482°	29.518°
EQ12	89.848°	179.848°
EQ13	89.319°	179.319°
EQ14	14.153°	75.847°
EQ15	71.499°	161.499°
Average	53.324°	106.799°

- There is a significant variation in the floor response spectrum of various locations on the same floor of AB due to uni-directional or bi-directional ground motion.
- The peak floor response varies from 16 % to 58 % of the lowest response on various locations of the same floor for uni-directional input motions.
- The peak floor response varies from 8 % to 30 % of the lowest response on various locations of the same floor for bi-directional input motions.
- The resultant peak floor responses due to bi-directional motion is 24 %–42 % larger than the respective responses due to uni-directional motion. It suggests that bi-directional motions should be considered to evaluate seismic behavior of a large irregular structure such as AB.
- The average peak resultant demands showed the critical angle of incidence for AB as 105°.

Based on the conclusion, it is suggested to consider seismic floor responses due to bi-directional ground motions to allocate various components of NPP.

CRediT authorship contribution statement

Bidhek Thusa: Writing – original draft, Formal analysis, Conceptualization. **Duy-Duan Nguyen:** Writing – review & editing, Validation, Data curation. **Md Samdani Azad:** Writing – review & editing, Data curation. **Tae-Hyung Lee:** Writing – review & editing, Supervision, Funding acquisition, Conceptualization.

Declaration of competing interests

The authors declare that they have no known competing financial interests or personal relationships that could have appeared to influence the work reported in this paper.

References

[1] V. Varma, G.R. Reddy, K.K. Vaze, H.S. Kushwaha, Simplified approach for seismic analysis of structures, Int. J. Struct. Stabil. Dynam. 2 (2) (2002) 207–225.
[2] I.K. Choi, Y.S. Choun, S.M. Ahn, J.M. Seo, Probabilistic seismic risk analysis of CANDU containment structure for near-fault earthquakes, Nucl. Eng. Des. 238 (6) (2008) 1382–1391.
[3] A. Ali, N.A. Hayah, D. Kim, S.G. Cho, Probabilistic seismic assessment of base-isolated NPPs subjected to strong ground motions of Tohoku earthquake, Nucl. Eng. Technol. 46 (5) (2014) 699–706.
[4] I. Zentner, Numerical computation of fragility curves for NPP equipment, Nucl. Eng. Des. 240 (6) (2010) 1614–1621.
[5] I. Zentner, N. Humbert, S. Ravet, E. Viallet, Numerical methods for seismic fragility analysis of structures and components in nuclear industry-Application to a reactor coolant system, Georisk 5 (2) (2011) 99–109.
[6] Y.N. Huang, A.S. Whittaker, N. Luco, A probabilistic seismic risk assessment procedure for nuclear power plants:(I) Methodology, Nucl. Eng. Des. 241 (9) (2011) 3996–4003.
[7] D.D. Nguyen, B. Thusa, T.H. Lee, Seismic fragility of base-isolated nuclear power plant considering effects of near-fault ground motions, Journal of the Korean Society of Hazard Mitigation 18 (7) (2018) 315–321.
[8] D.D. Nguyen, B. Thusa, T.H. Lee, Effects of significant duration of ground motions on seismic responses of base-isolated nuclear power plants, J. Earthq. Eng. Soc. Korea 23 (3) (2019) 149–157.
[9] D.D. Nguyen, B. Thusa, T.S. Han, T.H. Lee, Identifying significant earthquake intensity measures for evaluating seismic damage and fragility of nuclear power plant structures, Nucl. Eng. Technol. 52 (1) (2020) 192–205.
[10] B. Thusa, D.D. Nguyen, T.H. Lee, Seismic response evaluation of NPP structures considering different numerical models and frequency contents of earthquakes, J. Comput. Struct. Eng. Inst. Korea 33 (1) (2020) 63–72.
[11] J.W. Jung, H.W. Jang, J.H. Kim, J.W. Hong, Effect of second hardening on floor response spectrum of a base-isolated nuclear power plant, Nucl. Eng. Des. 322 (2017) 138–147.
[12] G.J. Kim, K.K. Yang, B.S. Kim, H.J. Kim, S.J. Yun, J.K. Song, Seismic response evaluation of seismically isolated nuclear power plant structure subjected to Gyeong-Ju earthquake, J. Earthq. Eng. Soc. Korea 20 (7) (2016) 453–460.
[13] J.H. Lee, J.K. Song, Seismic fragility analysis of seismically isolated nuclear power plant structures using equivalent linear-and bilinear-lead rubber bearing model, J. Earthq. Eng. Soc. Korea 19 (5) (2015) 207–217.
[14] S.H. Eem, H.J. Jung, M.K. Kim, I.K. Choi, Seismic fragility evaluation of isolated NPP containment structure considering soil-structure interaction effect, J. Earthq. Eng. Soc. Korea 17 (2) (2013) 53–59.
[15] E.H. Lee, J.M. Kim, K.H. Joo, H.U. Kim, Evaluation of the soil-structure interaction effect on seismically isolated nuclear power plant structures, J. Earthq. Eng. Soc. Korea 20 (6) (2016) 379–389.
[16] S.G. Cho, D. Kim, S. Chaudhary, A simplified model for nonlinear seismic response analysis of equipment cabinets in nuclear power plants, Nucl. Eng. Des. 241 (8) (2011) 2750–2757.
[17] S.H. Eem, I.K. Choi, Seismic response analysis of nuclear power plant structures and equipment due to the pohang earthquake, J. Earthq. Eng. Soc. Korea 22 (3) (2018) 113–119.
[18] J.B. Park, N.C. Park, S.J. Lee, Y.P. Park, Y. Choi, Seismic analysis of the APR1400 nuclear reactor system using a verified beam element model, Nucl. Eng. Des. 313 (2017) 108–117.

[19] H. Lee, Y.C. Ou, H. Roh, J.S. Lee, Simplified model and seismic response of integrated nuclear containment system based on frequency adaptive lumped-mass stick modeling approach, KSCE J. Civ. Eng. 19 (6) (2015) 1757–1766.

[20] S. De Grandis, M. Domaneschi, F. Perotti, A numerical procedure for computing the fragility of NPP components under random seismic excitation, Nucl. Eng. Des. 239 (11) (2009) 2491–2499.

[21] V. Jussila, Y. Li, L. Fülöp, Statistical analysis of the variation of floor vibrations in nuclear power plants subject to seismic loads, Nucl. Eng. Des. 309 (2016) 84–96.

[22] J. Hur, E. Althoff, H. Sezen, R. Denning, T. Aldemir, Seismic assessment and performance of nonstructural components affected by structural modeling, Nucl. Eng. Technol. 49 (2) (2017) 387–394.

[23] G. Dundulis, R. Kačianauskas, D. Markauskas, E. Stupak, S. Stupak, S. Šliaupa, Reanalysis of the floor response spectra of the ignalina nuclear power plant reactor building, Nucl. Eng. Des. 324 (2017) 260–268.

[24] H.P. Lee, Shell finite element of reinforced concrete for internal pressure analysis of nuclear containment building, Nucl. Eng. Des. 241 (2) (2011) 515–525.

[25] N. Nakamura, N. Yabushita, T. Suzuki, J. Yamada, N. Tsunashima, T. Nakano, Analyses of reactor building by 3D nonlinear FEM models considering basemat uplift for simultaneous horizontal and vertical ground motions, Nucl. Eng. Des. 238 (12) (2008) 3551–3560.

[26] N. Nakamura, S. Akita, T. Suzuki, M. Koba, S. Nakamura, T. Nakano, Study of ultimate seismic response and fragility evaluation of nuclear power building using nonlinear three-dimensional finite element model, Nucl. Eng. Des. 240 (1) (2010) 166–180.

[27] Y.J. Zhang, Finite element analysis of a containment vessel structures based on the multi-layer shell elements, in: Applied Mechanics and Materials, vol. 711, Trans Tech Publications Ltd, 2015, pp. 82–85.

[28] W. Chao, The applicability study on the multi-layer shell element method in steel concrete structure of shield building, in: 2017 25th International Conference on Nuclear Engineering, American Society of Mechanical Engineers Digital Collection, 2017.

[29] D.K. Thai, S.E. Kim, Safety assessment of a nuclear power plant building subjected to an aircraft crash, Nucl. Eng. Des. 293 (2015) 38–52.

[30] Z.R. Li, Z.C. Li, Z.F. Dong, T. Huang, Y.G. Lu, J.L. Rong, H. Wu, Damage and vibrations of nuclear power plant buildings subjected to aircraft crash part II: numerical simulations, Nucl. Eng. Technol. 53 (9) (2021) 3085–3099.

[31] D.A. Pecknold, Inelastic structural response to 2D ground motion, J. Eng. Mech. Div. 100 (5) (1974) 949–963.

[32] T. Hisada, M. Miyamura, S. Kan, Y. Hirao, Studies on the orthogonal effects in seismic analyses, in: Proc., *9th World Conf. On Earthquake Engineering*, A.A. Balkema, Rotterdam, Netherlands, 1988.

[33] M. Çelebi, Response of olive view hospital to Northridge and Whittier earthquakes, J. Struct. Eng. 123 (4) (1997) 389–396.

[34] M.M. Hachem, J.P. Moehle, S.A. Mahin, Performance of circular reinforced concrete bridge columns under bidirectional earthquake loading. Pacific Earthquake Engineering Research Center, 2003. Berkeley, CA.

[35] J.C. Reyes, E. Kalkan, Should ground-motion records be rotated to fault-normal/parallel or maximum direction for response history analysis of buildings, US Geological Survey Open-File Report 1261 (2012) 89, 2012.

[36] Y.N. Huang, A.S. Whittaker, N. Luco, Maximum spectral demands in the near-fault region, Earthq. Spectra 24 (1) (2008) 319–341.

[37] T.T. Tran, T.H. Nguyen, D. Kim, Seismic incidence on base-isolated nuclear power plants considering uni-and bi-directional ground motions, J. Struct. Integr. Mainten. 3 (2) (2018) 86–94.

[38] Y. Lin, X. He, A. Igarashi, Influence of directionality of spectral-compatible Bi-directional ground motions on critical seismic performance assessment of base-isolation structures, Earthq. Eng. Struct. Dynam. 51 (6) (2022) 1477–1500.

[39] SAP2000, C. S. I., Computers and Structures Inc, 2013. Berkeley, CA, USA.

[40] Z.W. Miao, X.Z. Lu, J.J. Jiang, L.P. Ye, Nonlinear FE model for RC shear walls based on multi-layer shell element and microplane constitutive model, Computational Methods in Engineering and Science (2006) 21–23.

[41] Y.M. Fahjan, J. Kubin, M.T. Tan, Nonlinear analysis methods for reinforced concrete buildings with shear walls, in: 14th European Conference on Earthquake Engineering, 2010.

[42] X. Lu, L. Xie, H. Guan, Y. Huang, X. Lu, A shear wall element for nonlinear seismic analysis of super-tall buildings using OpenSees, Finite Elem. Anal. Des. 98 (2015) 14–25.

[43] B. Thusa, Seismic Interaction of Adjacent Main NPP Buildings under Bi-directional Ground Motions [Doctoral Dissertation, Konkuk University, 2024. http://konkuk.dcollection.net/common/orgView/200000725401.

[44] NRC 1.60, Regulatory Guide 1.60: Design Response Spectra for Seismic Design of Nuclear Power Plants, US Nuclear Regulatory Commission, Rockville, 1973. Maryland, USA.

[45] NRC, US Nuclear Regulatory Commission 1.60: Design Response Spectra for Seismic Design of Nuclear Power Plants, 2014. Regulatory Guide 1.60, Revision 2, Rockville, Maryland, USA.

[46] PEER center, PEER Ground Motion Database, Pacific Earthquake Engineering Research Center, University of California, Berkeley, CA, USA, 2020. http://ngawest2.berkeley.edu.